



# Dissolution of cotton by 1-ethyl-3-methylimidazolium acetate studied with time–temperature superposition for three different fibre arrangements

Yunhao Liang · James E. Hawkins · Michael E. Ries · Peter J. Hine

Received: 3 September 2020 / Accepted: 5 November 2020 / Published online: 19 November 2020  
© The Author(s) 2020

**Abstract** This study has investigated the dissolution of cotton fibres in the ionic liquid 1-ethyl-3-methylimidazolium acetate ([C2mim][OAc]) for three fibre arrangements. Dissolution was carried out with excess [C2mim][OAc] at various temperatures and times followed by coagulation with water. Optical microscopy (OM) of the resulting processed and dried cotton fibres indicated that this procedure produced a coagulated fraction surrounding the original fibres. X-ray diffraction (XRD) showed that the crystal structure of this coagulated fraction was predominantly cellulose II, as opposed to the original fibres—

mostly cellulose I. The OM and XRD results showed that growth of the coagulated fraction obeyed time–temperature superposition (TTS) and displayed an Arrhenius behaviour allowing a dissolution activation energy to be determined. Although the growth of the coagulated fraction with time were different for these distinct three arrangements, all could be individually shifted to form master curves using TTS, leading to very similar activation energies,  $96 \pm 3$  kJ/mol ( $23 \pm 1$  kcal/mol).

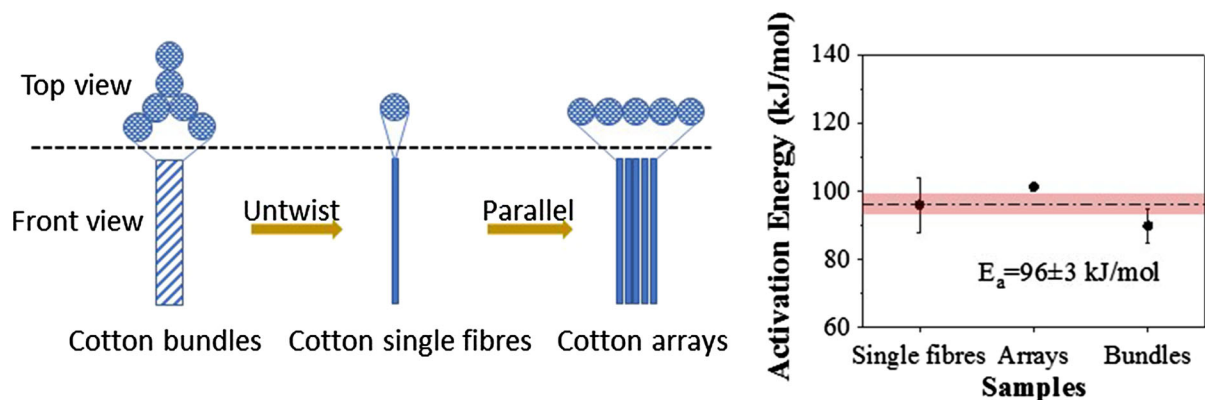
---

**Electronic supplementary material** The online version of this article (<https://doi.org/10.1007/s10570-020-03576-x>) contains supplementary material, which is available to authorized users.

---

Y. Liang · J. E. Hawkins · M. E. Ries (✉) · P. J. Hine  
School of Physics and Astronomy, University of Leeds,  
Woodhouse Lane, Leeds LS2 9JT, UK  
e-mail: M.E.Ries@leeds.ac.uk

## Graphic abstract



**Keywords** Cellulose · Ionic liquid · Activation energy · TTS

## Introduction

Cellulose is the most abundant and renewable natural biopolymer on earth and due to its particular molecular structure has unique chemical and physical properties, such as high thermostability and excellent mechanical capabilities (Nishino et al. 1995; Zhang et al. 2017). Therefore, cellulose has gained increasing attention as a replacement material for a number of finite fossil fuel products (Jiang et al. 2019; Sayyed et al. 2019). Due to the highly crystalline structure, abundant intra and intermolecular hydrogen bonds and the hydrophobic interactions between rings, cellulose is insoluble in water and in most organic solvents. It can only be dissolved via the breaking down of the hydrogen bond network (Glasser et al. 2012; Lindman et al. 2010).

Cellulose can be dissolved via two key ways, either with prior chemical modification or without (Sen et al. 2013). For the former, the hydroxyl groups on the cellulose molecules are firstly functionalized, by nitration for example (Barbosa et al. 2005), esterification (Ratanakamnuan et al. 2012), etherification (Fox et al. 2011) or xanthation (Polyuto et al. 2000). In general, these processes are environmentally harmful (Zhang et al. 2017). For example, the first industrialized procedure for fabricating rayon fibres, known as the viscose process, uses carbon disulphide and aqueous sodium hydroxide; both of which are known to be environmentally damaging. The production of

sodium cellulose xanthate involves harmful chemicals such as sulphuric acid,  $H_2S$  and  $SO_2$  (Clotworthy 1928). For the later method (without chemical modification), solvents such as N-methylmorpholine-N-oxide monohydrate (NMMO) (Rosenau et al. 2002), Lithium Chloride/N, N-Dimethylacetamide (LiCl/DMAc) (Matsumoto et al. 2001), Sodium Hydroxide (NaOH) Aqueous Solution (Cai et al. 2007), etc. can dissolve cellulose by breaking the hydrogen bonds directly. These solvents however also have several disadvantages, such as: high vapour pressure; low thermostability; and a high level of toxicity. The only commercialized solvent, NMMO, cannot be considered environmentally-friendly due to the combination of the oxidative side reactions, difficulty to recycle and high temperatures needed for dissolution (Rosenau et al. 2002).

As a result of the increasing demand for ‘green’ cellulose solvents, ionic liquids (ILs) containing anions and cations have gained attention as promising cellulose solvents due to their high thermostability, negligible vapor pressure, broad liquid applied range, designable properties and potential recyclability (Seoud et al. 2007; Moon et al. 2011). The history of the application of ILs for dissolving cellulose can be traced back to a patent in 1934, (Graenacher 1934) though their popularity as green solvents was initiated more recently when Swatloski et al. (2002) discovered the efficacy of dialkylimidazolium-based ILs (with melting points below 100 °C) as suitable solvents for cellulose (Swatloski et al. 2002). This original work has led to an increasing interest in ILs in relation to cellulosic dissolution. To date, cellulose with solubility up to 39% dissolving in 3-methyl-N-

butylpyridinium chloride has been reported (Heinze et al. 2005). Once dissolved, cellulose can then be coagulated from the viscous cellulose-ILs solution by coagulation in agents such as water, ethanol and acetone. This is followed by a drying process to evaporate the coagulants (Huber et al. 2012). The mechanism by which coagulation occurs can be explained as follows: coagulants stop the dissolving process via the preferential breaking of hydrogen bonds between solvent molecules and cellulose molecules, forming new hydrogen bonds between the solvent and coagulant molecules (Gupta et al. 2013).

It is important to understand and quantify the cellulose dissolution behaviour in ILs for both chemical derivatization and other cellulose processing methods. The mechanism by which ILs dissolve cellulose is still not fully understood, but the most widely accepted hypothesis is that the anions in the ionic liquids play a predominant role—by competing with the hydroxyl groups on the cellulose to form new hydrogen bonds. Additionally, it is thought the cations play a minor role in the solvation of cellulose (Cho et al. 2011; Lu et al. 2014; Zhang et al. 2017). As reported by Cuissinat et al. (2008), there are four possible states, observable via optical microscopy, by which cellulose fibres can exist during dissolution in ionic liquids. These states are as follows: state 1, balloon formation (due to the swelling of cellulose); state 2, bursting of this balloon; state 3, dissolution of the unswollen areas; state 4, dissolution of the balloon membrane.

A number of authors have reported on the kinetics of cellulosic dissolution in ionic liquids (Budtova and Navard 2015; Druel et al. 2018; Gericke et al. 2009). Within these studies, a rheological activation energy, ranging from 46 kJ/mol to approximately 70 kJ/mol, is documented. This energy is shown to be dependent on the IL used and the concentration of cellulose. Additionally, a recently published paper showed that the dissolution rate of cellulose fibers was in linear correlation with the viscosity of 1-ethyl-3-methylimidazolium acetate ([C2mim][OAc]) when both are expressed in natural logarithmic form. Furthermore, the dissolution process was found to follow Arrhenius behaviour (Chen et al. 2020). A number of other authors have studied the thermodynamics of dissolution, as well as the dissolution enthalpies of cellulose in multiple ILs; which were found to be dependent on

the water content of the ILs, anion-cation composition and cellulose source (Parviainen et al. 2014). Moreover, the enthalpy of solvation of a cellulose pentamer in [C2mim][OAc] was reported to be 96.4 kJ/mol, which was obtained from force-field molecular dynamics simulations (Brehm and Pulst 2019). Even though there have been some research on the cellulose/ILs solution, the cellulose dissolution behaviour in ILs still needs to be further quantified.

In this current work, investigation of the dissolution behaviour of cellulose in ILs is conducted using a combination of X-ray diffraction (XRD) and optical microscopy (OM). Both techniques allow for the growth of the dissolved and coagulated fraction (CF) at various temperatures and times to be quantitatively measured. Cotton was chosen to be the source of cellulose, displaying the highest cellulose I content of all plants, at around 90%. The IL chosen was [C2mim][OAc], which is a liquid at room temperature and has been widely studied within our research group (Green et al. 2017; Lovell et al. 2010; Ries et al. 2014; Sescousse et al. 2010). The effect of different cotton fibre arrangements including single fibres, arrays and bundles on dissolution in [C2mim][OAc] is studied with time–temperature superposition (TTS). The cellulose dissolution behaviour is also quantified by the determination of an activation energy of dissolution for each cotton fibre arrangement. Additionally, the effect of cotton fibre arrangement on dissolution speed is also investigated. Apart from providing quantitative information on the physics of cellulose dissolution, we believe that the results of this study will aid in future research in relation to the production of all-cellulose composites (Gindl and Keckes 2005; Nishino et al. 2004). Within these materials, any of the fibre arrangements used in this study may be utilised.

## Materials and methods

### Materials

Undyed cotton yarn (obtained from Airedale Yarns, Keighley, UK) was used as the source of the cellulose. 1-ethyl-3-methylimidazolium acetate ([C2mim][OAc]) with purity  $\geq 95\%$  was purchased from Sigma-Aldrich Corporation. The water content was always below 0.5 wt. % in the experiments as determined by quantitative NMR. Epoxy (Epoxicure, Cold Cure Mounting Resin

from Buehler, UK) was used to embed samples for optical microscopy.

## Methods

### *The processing of cotton samples with [C2mim][OAc]*

The natural undyed cotton yarn was supplied in the form of a bundle of six fibres, as shown on the left in Fig. 1. A single fibre was obtained by untwisting the bundle, while the parallel array was formed by closely packing 30 single (untwisted) fibres together (Fig. 1 right).

For single fibre experiments, the untwisted cotton was wound around a Teflon picture frame. Five fibre loops were put onto the frame (Fig. 2) in order to give multiple samples for testing, which were processed under the same processing conditions. The array was made by aligning 30 turns of single fibres next to each other on one side of the frame, also shown in Fig. 2. Upon fixing all fibers to the frame, the frame was then submerged in a Teflon dish fully filled with approximately 50 mL of [C2mim][OAc]. The [C2mim][OAc] was preheated at the target temperature in an oven for 50 min. This combination of cotton and IL gave a solid to liquid mass ratio of approximately 1–40, in which the [C2mim][OAc] was in excess (Le et al. 2014). Immediately after submersion, the dish with samples was put into a vacuum oven (Shellab 17L Digital Vacuum Oven SQ-15VAC-16, Sheldon Manufacturing, Inc., USA) in order to

dissolve cotton samples at different temperatures and for different times whilst under vacuum. A water bath was then used to coagulate the cotton samples after being taken out from the solvent. The coagulating process took place beneath a tap of running water and lasted for 24 h to remove all the solvent. A drying process then followed at 120 °C for 1 h under vacuum. For the cotton bundles, the dissolving procedure was same as for single fibres and arrays, but cotton bundles were wound on the frame by 5 turns, each separate to each other.

Samples are labelled in the following way in this work: processed samples were named CF-x-y, CB-x-y and CA-x-y, which represent a single cotton fibre, a cotton bundle and cotton array processed at temperature ‘x’ (°C) for ‘y’ hours. Single fibres, arrays and bundles are illustrated in Fig. 1.

### *Optical microscopy*

An optical microscope (BH2-UMA, Olympus Corporation, Japan) was used in reflection mode to explore the micromorphology of the cotton samples before and after processing at different dissolving temperatures and times. Each set of three samples were embedded in an epoxy resin and polished down to the surface in order to allow the morphology to be investigated. The image processing software ‘ImageJ 1.52d’ was used to measure the areas of different sections of the processed samples, including the total cross section area

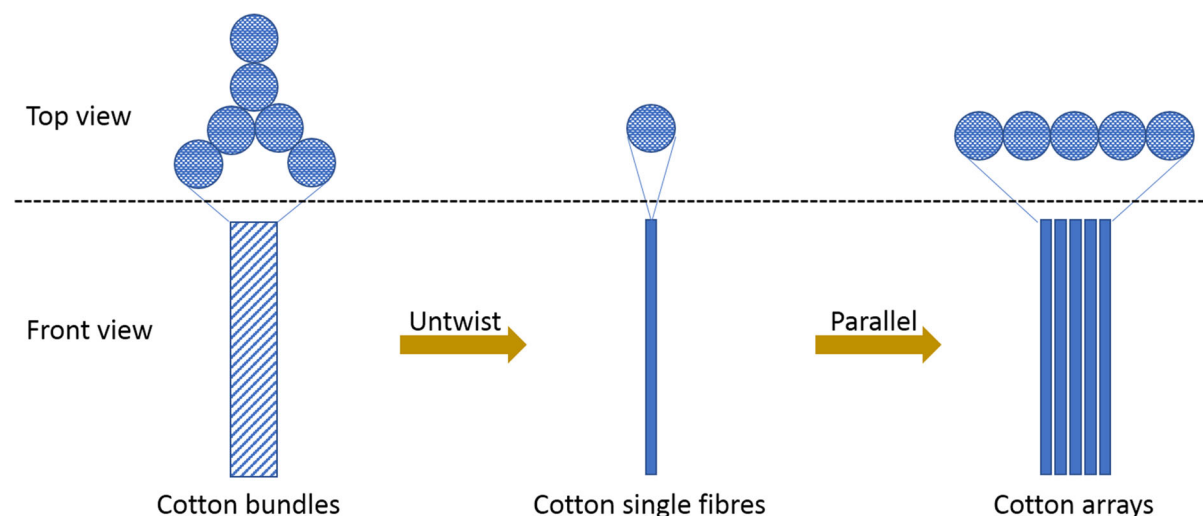


**Fig. 1** The three cotton fibre arrangements studied in this work



where  $A_{red}$  and  $A_{blue}$  represent the area of the coagulated material and the area of the central fibre as shown in Fig. 3.

### X-ray diffraction

X-ray Diffraction (XRD) was applied to characterize the crystalline structure of samples on a XRD machine (DRONEK 4-AXES, Huber Diffractionstechnik GmbH & Co. KG, Germany) under transmission mode.  $2\theta$  scans were used to characterise the samples using the following settings:  $2\theta$  from  $5^\circ$  to  $40^\circ$ ; step to be  $0.2^\circ$  for 50 s per step; X-ray generated by Cu-K $\alpha$  at 40 kV and 30 mA with wavelength ( $\lambda$ ) to be 0.154 nm. The intensity vs.  $2\theta$  curves were obtained by subtraction of the background by scanning without loading any sample and the Cellulose I fraction was calculated by a deconvolution method. Peaks at  $14.8^\circ$ ,  $16.3^\circ$ ,  $20.6^\circ$  and  $22.4^\circ$  on  $2\theta$  are considered to belong to Cellulose I structure and those at  $12.4^\circ$ ,  $20.2^\circ$  and  $21.8^\circ$  are from Cellulose II structure (Liu et al. 2012). There is also a broad peak centred at an angle of  $18.2^\circ$  of  $2\theta$ , which belongs to the amorphous fraction (Liu et al. 2012).

Due to the fact that the conversion from Cellulose I to Cellulose II is irreversible, the coagulation fraction based on the XRD spectrums,  $CF_{XRD}$ , can be calculated according to the difference in the Cellulose I fraction before and after processing:

$$CF_{XRD} = (C_0 - C')/C_0 \quad (2)$$

where  $C_0$  and  $C'$  stand for the total Cellulose I content in the raw cotton sample and the processed cotton sample respectively.

## Results and discussion

### Micromorphology

Typical optical micrographs of cotton single fibres (CF) and cotton bundles (CB) processed at different temperatures and times are shown in Fig. 4.

As shown in Fig. 4a, the unprocessed single cotton fibre consists of a loose arrangement of many smaller cotton microfibrils, each with a diameter of around 13  $\mu\text{m}$ . The processed single fibres, seen in Fig. 4b–g, were much smaller in diameter. This is likely due to

the expansion of the fibre composed of non-bonded filaments in the raw cotton sample by the epoxy resin. Examination of the micrographs suggest that there was minimal cellulose dissolved in the central fibre area, suggesting that the processed fibres can be viewed as a composite material—comprised of a central core surrounded by a coagulated fraction.

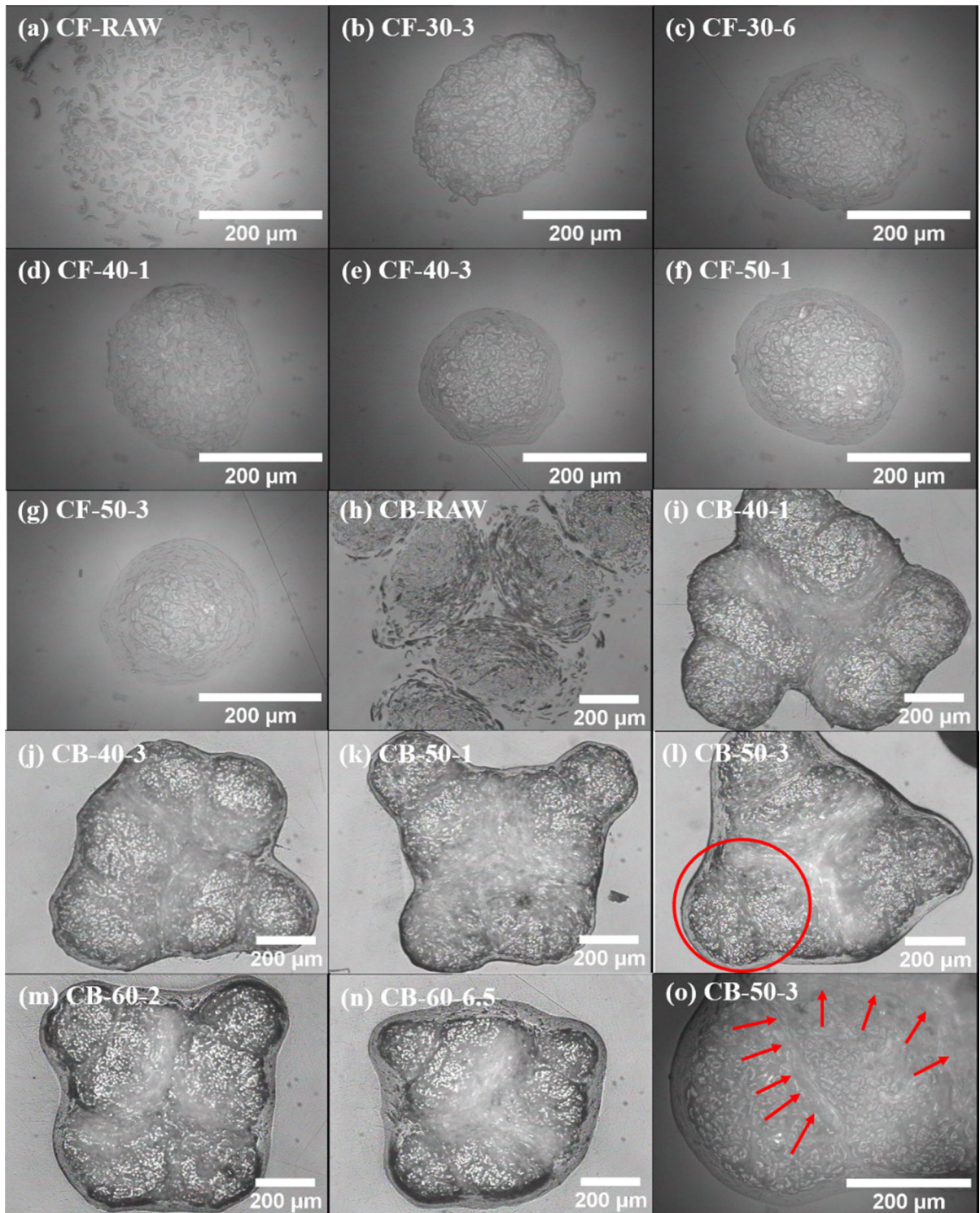
For the cotton bundles, as shown in Fig. 4h there are six single cotton fibres in one cotton bundle and due to this arrangement, the dissolution occurred not only at the perimeter of the samples, but also in the central fibre area. This is shown in Fig. 4o, which is a magnified view of the circled area in Fig. 4l, in which the coagulated fraction is shown by the arrows.

Both the cotton single fibres and cotton bundles display the ring-like outer coagulation fraction, which increases in size in line with increasing temperature and/or time. Equation (1) however, is only valid in describing the CF of the single fibres. This is because the central area of the cotton bundles contains some partially dissolved cellulose which cannot be measured by optical microscopy. Therefore, X-ray diffraction was also used to determine the growth of the coagulation fraction for both arrays and bundles.

### Dissolution of cotton single fibres in [C2mim][OAc] analysed using Arrhenius dependence

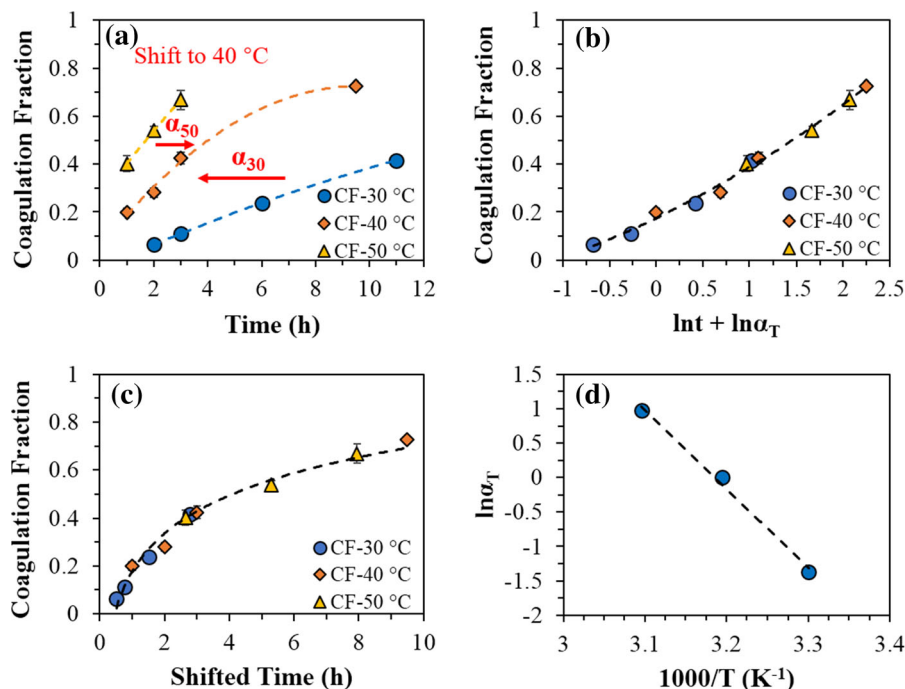
The coagulation fraction of single fibres processed at different temperatures and times was measured by optical microscopy, see Fig. 4, and calculated with Eq. (1), the results of which are shown in Fig. 5a.

Figure 5a shows how the coagulation fraction increases with both the processing time and the processing temperature. This is consistent with what was observed via the optical microscope images in Fig. 4. Examination of the curves in Fig. 5a suggested that a time–temperature equivalence could be applied in order to create a master curve at each specific temperature, as is routinely done in rheological analysis. The process used to obtain a master curve at  $40^\circ\text{C}$  was as follows: Firstly, the data points attained at  $40^\circ\text{C}$  were chosen to be the reference set with a shift factor ( $\alpha_{40} = 1$ ), as shown in Fig. 5a. Next, the x-axis was converted from time,  $t$ , to natural logarithmic time,  $\ln(t)$  and the  $40^\circ\text{C}$  data was fitted with a preliminary polynomial function in order to provide a visual guide for further shifting. After this,



**Fig. 4** Optical microscope pictures of cotton single fibres (CF) from **a–g** and cotton bundles (CB) from **h–o** processed at different temperatures for different times with scale bars

indicating 200 microns. Image **(o)** is a magnification of the area enclosed within the red circle in **l**, in which the arrows point to the coagulated area



**Fig. 5** a Coagulation fraction dependence of time for cotton single fibres (CF) and the time–temperature superposition plot after being shifted to 40 °C on both **b** natural-logarithmic time scale and **c** linear time scale; **d** Arrhenius plot with  $R^2 > 0.99$

each other temperature dependant data set was horizontally shifted by a number equal to  $\ln(\alpha_T)$  towards the reference data by eye, before fitting all data points with a final polynomial function. Finally, the  $R^2$  value of the final fitting polynomial function was maximized by adjusting the shift factors  $\alpha_T$  at 30 °C and 50 °C ( $\alpha_{30}$  and  $\alpha_{50}$ ).

Figure 5b shows the optimised polynomial master curve (at 40 °C) in natural logarithmic time, while Fig. 5c shows the same data in linear time. It can be seen that the individual results from Fig. 5a form a convincing master curve, providing evidence of the proposed interchangeability between time and temperature. The results show that the dissolution speed is initially quite fast and then slows down as time progresses.

Plotting the  $\ln$  of the shift factors versus the inverse temperature results in a linear plot, indicating that the dissolution dynamics follow Arrhenius behaviour. This allows the activation energy for the process to be calculated using the Arrhenius equation,

$$\ln \alpha_T = A + E_a/RT \quad (3)$$

where  $E_a$ ,  $A$ ,  $R$  and  $T$  represent activation energy, Arrhenius prefactor, gas constant and temperature respectively.  $\alpha_T$  represents the shift factor at temperature  $T$ .

The resulting time–temperature superposition and Arrhenius plot are shown in Fig. 5c and d respectively. The activation energy associated with the dissolution of a single cotton fibre in [C2mim][OAc] was calculated from the slope of Fig. 5d to be  $96 \pm 8$  kJ/mol. This value compares with reported rheological activation energies ranging from 46 kJ/mol to about 70 kJ/mol (Budtova and Navard 2015; Druel et al. 2018; Gericke et al. 2009) and the flax dissolution activation energy of  $98 \pm 2$  kJ/mol in [C2mim][OAc] reported by Hawkins et al. (Hawkins et al. 2020). The rate of increase of the coagulation fraction was seen to fall with increasing time, as seen from the master curve (Fig. 5c). One hypothesis is that as the processing time is increased, more and more of the outer cellulose is dissolved which in turn may act as a protective barrier between the inner core and exterior solvent.

## Crystalline structure of cotton arrays and cotton bundles

In order to determine the crystalline structure, amount of crystallinity and the coagulation fraction, XRD was used on both cotton arrays and bundles. See Fig. SI 1, the raw cotton sample was found to be composed of 71% Cellulose I and 29% amorphous material, which was determined via the deconvolution of the XRD spectrum in Fig. 6. Upon processing of both the cotton arrays and bundles, the ratio of the Cellulose I peaks, especially the main reflection at  $22.4^\circ$  (200), to the amorphous peak at  $18.2^\circ$  was seen to decrease and the crystalline structure showed a conversion from Cellulose I to Cellulose II, seen most notably by the shifting of the main cellulose I peak at  $22.4^\circ$  to the dominant cellulose II peak at  $20.2^\circ$ . The increasing of both time and/or temperature resulted in a more significant crystalline structure conversion from cellulose I to cellulose II. Figure 6a, b and c show the XRD scans for a range of times at processing temperatures  $30^\circ\text{C}$ ,  $40^\circ\text{C}$  and  $50^\circ\text{C}$  respectively. A good indication of the amount of dissolution is given by the relative size of the double peak at around  $15^\circ$  in  $2\theta$ , which is a

convolution of the  $1\bar{1}0$  ( $14.8^\circ$ ) and  $110$  ( $16^\circ$ ) reflections of the cellulose I crystal, with no notable cellulose II reflections seen at these angles. At a processing temperature of  $50^\circ\text{C}$ , these two reflections were markedly lower, suggesting a significantly increased speed of dissolution and a greater level of transformation from Cellulose I to Cellulose II.

As shown from graphs in Fig. 6c and d, the cotton bundles dissolve far more slowly—as is evident by the lack of change from a cellulose I to cellulose II signal. Even after 11 h at  $50^\circ\text{C}$ , the bundles still show a strong cellulose I peak at  $22.4^\circ$ .

## Analysis of dissolution of cotton arrays and cotton bundles using time–temperature superposition

The coagulation fraction of the cotton arrays and cotton bundles was calculated using Eq. (2) in conjunction with the Cellulose I content obtained from the deconvolution of XRD data. The coagulation fraction as a function of both processing time and temperature is shown in Fig. 7.

As shown in Fig. 7a and c, the coagulation fraction of both cotton arrays and bundles shows a similar

**Fig. 6** XRD spectrums of cotton arrays (CA) processed at **a**  $30^\circ\text{C}$ , **b**  $40^\circ\text{C}$  and **c**  $50^\circ\text{C}$ , and **d** cotton bundles (CB) processed at  $50^\circ\text{C}$  for different times

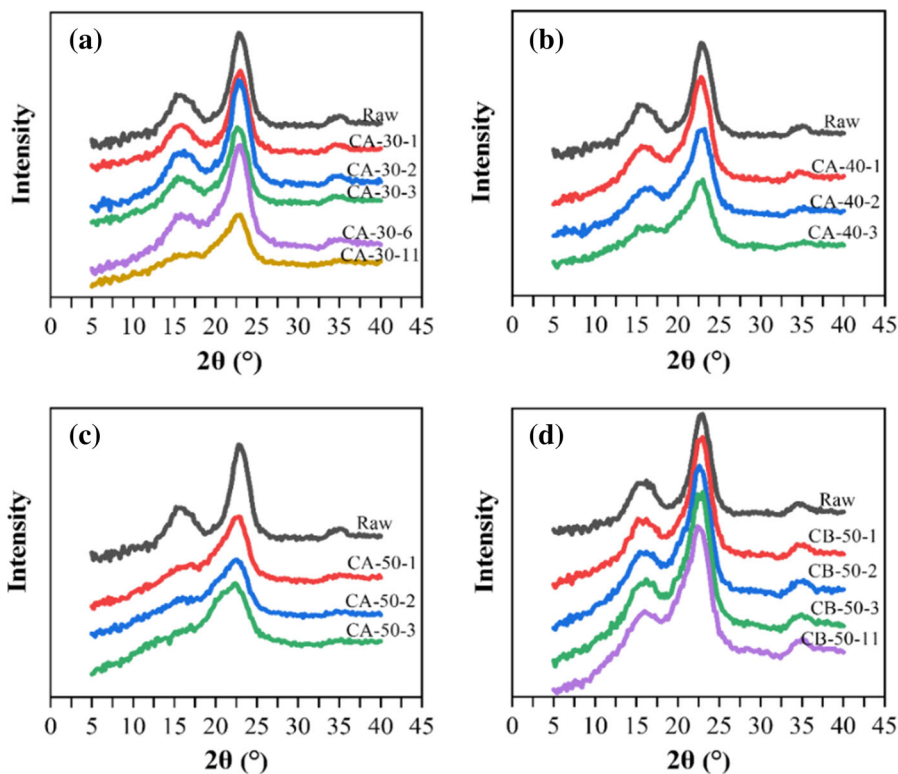
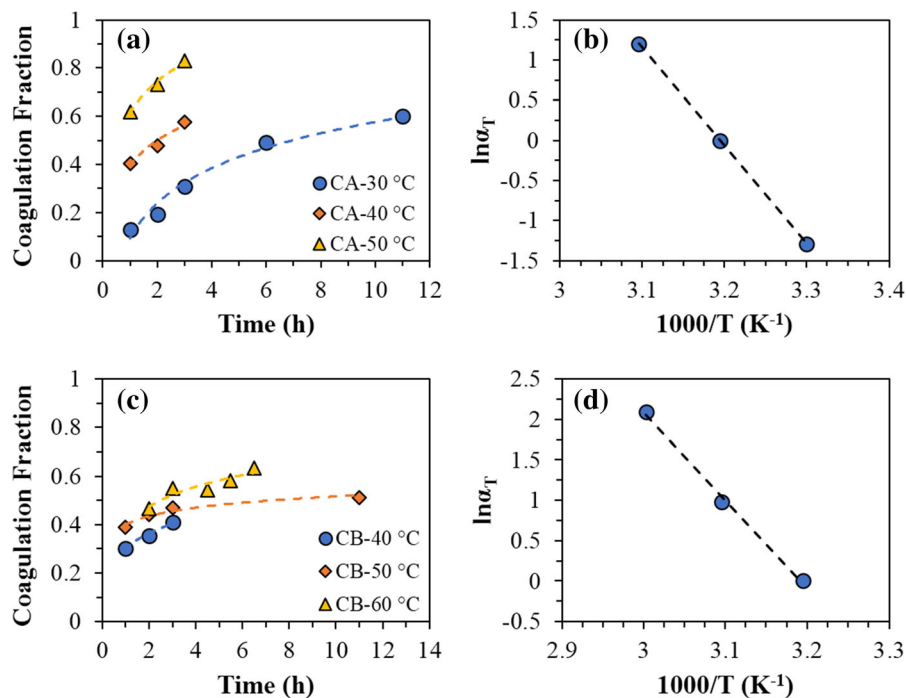


**Fig. 7** Coagulation fraction as a function of dissolution time and temperature for **a** cotton arrays (CA) and **c** cotton bundles (CB); Arrhenius plot of **b** cotton arrays (CA) and **d** cotton bundles (CB) with  $R^2 > 0.99$



dependence on processing time and temperature as the single cotton fibres (Fig. 5a). Compared with cotton bundles, the cotton arrays dissolved faster with increased temperature, as evident by a higher coagulation fraction at higher temperatures for the same dissolution time. These results are in close agreement with the observed XRD patterns described above. That is, the crystalline structure is converted from cellulose I to cellulose II in accordance with increasing dissolution time and/or temperature. This conversion is again slower for the cotton bundles.

Time–temperature superposition was again used in order to obtain a master curve for the arrays and bundles using the same procedure as is outlined in a previous section. Figure 7b and d show Arrhenius plots in relation to the dissolution of both arrays and bundles respectively. The corresponding activation energies are calculated from the gradients and are found to be  $101.3 \pm 0.2$  kJ/mol (arrays) and  $90 \pm 5$  kJ/mol (bundles).

Comparison of the dissolution behaviour among all three fibre arrangements

In order to analyse the effect of the arrangement of fibres on the dissolution behaviour, the activation

energy vs. sample type (single fibres/arrays/bundles) and a time–temperature superposition plot, including data from all sample types were plotted and are shown in Figs. 8 and 9 respectively.

It can be seen from Fig. 8 that the three cotton samples all have very similar activation energies, with

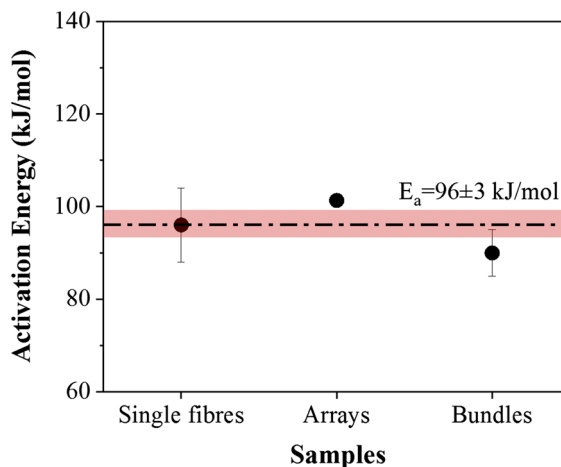


**Fig. 8** Comparison of activation energies for cotton single fibres, arrays and bundles. the dot-dashed line indicates position of the average value and the rectangular shape indicates the error margin. For the arrays, the error bar is smaller than the size of symbol used

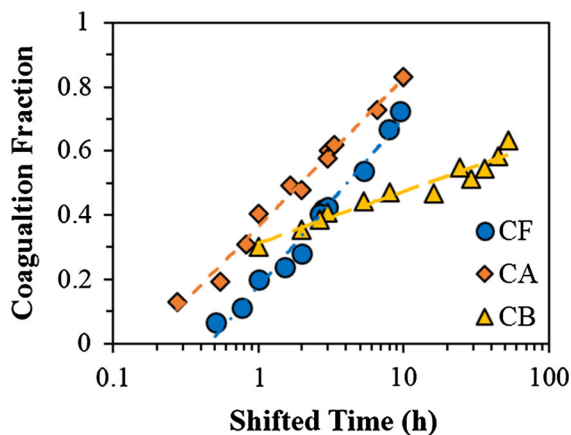


**Fig. 9** Comparison of time–temperature superposition after being shifted to 40 °C among cotton single fibres (CF), cotton arrays (CA) and cotton bundles (CB)

an average value of  $96 \pm 3$  kJ/mol. This result, quite surprisingly, suggests that the arrangement of the cotton fibres has no influence on the dissolution activation energy within the errors of these three measurements.

The dissolving speed of different cotton samples is compared in Fig. 9, whereby the three cotton samples' time–temperature superposition master curves at a reference temperature of 40 °C are combined in the same plot. Recall, these master curves describing the growth of the coagulation fraction with time were determined via two different techniques: optical microscopy for the single cotton fibres and x-ray deconvolution for the cotton arrays and the cotton bundles. It is seen that the dissolution speed of the cotton single fibres and cotton arrays is quite similar, despite the different experimental methods used to arrive at these results.

Figure 9 also shows that the cotton fibre bundles dissolved much more slowly than the other two fibre arrangements. It could be proposed that once the interior of the cotton fibre bundles is full of dissolved cellulose, the IL can then only access the outer surface of the bundles, resulting in a slower increase in CF. The final dissolution speed ranking is:  $CA \approx CF > CB$  which shows that cotton fibre arrangement plays an important role in dissolution rate of cotton samples with excess [C2mim][OAc]. These findings could be useful to future studies on the manufacturing of cotton fibre based, all cellulose composites.

## Conclusions

The dissolution behaviour of cotton fibres in the ionic liquid [C2mim][OAc] has been studied using X-ray diffraction and optical microscopy. Different arrangement of cotton fibres were processed with [C2mim][OAc] at different temperatures for a range of times, after which XRD and optical microscopy were used for characterizing the crystalline structure and micromorphology of the samples. The amount of dissolution was quantified by calculating the coagulation fraction from either optical microscopy pictures of processed fibre cross sections, or X-ray diffraction deconvolution by which the cellulose I fraction was obtained. The growth of the coagulated fraction was found to follow time–temperature superposition and an Arrhenius behaviour was found for the shift factors used  $\alpha_T$ . OM pictures show that the cotton single fibre was dissolved from the outer layer with a coagulation layer forming around the undissolved central core. As either time and/or temperature was increased the coagulation layer became larger. For arrays and bundles, the dissolution also happens in-between different single fibres, which makes the quantifying method for single fibres from OM pictures unsuitable to arrays and bundles. Therefore, the decrease of Cellulose I measured from XRD was chosen to calculate the coagulation fraction for both cotton bundles and arrays, see Eq. (2). XRD results show that the raw cotton samples are native cellulose with a Cellulose I fraction of 71% which transforms to Cellulose II after processing, in other words the outer coagulation layer of processed cotton single fibre can be considered to be Cellulose II and amorphous cellulose. Compared with cotton bundles, cotton arrays dissolve at a faster rate as shown in Fig. 9. The kinetics of cellulose dissolution is quantified by an activation energy calculated from an Arrhenius equation. For single fibres, arrays and bundles, the dissolution activation energies are  $96 \pm 8$  kJ/mol,  $101.3 \pm 0.2$  kJ/mol and  $90 \pm 5$  kJ/mol, respectively. These activation energies show an independence of the cotton fibre arrangement and are all in a good agreement with an average value of  $96 \pm 3$  kJ/mol ( $23 \pm 1$  kcal/mol). In contrast, the dissolution speed is influenced by cotton fibre arrangement significantly, with a ranking of:  $CA \approx CF > CB$ . The methods and results presented in this work could be instructive for the further study of the dissolution of cellulose-based

materials and the fabrication of cotton-based all cellulose composites, which could be made from woven cotton fibres or bundles.

**Acknowledgments** The authors would like to thank Dr. Daniel L. Baker, Experimental Officer in the school of Physics and Astronomy, University of Leeds for the experiment training and instruction. Xin Zhang and Maer Hael are also thanked for their contribution at discussions during the progress of this research.

**Author's contribution** All authors contributed to the study conception and design. Material preparation, data collection and analysis were mainly performed by YL under supervisions from MER and PJH. The first draft of the manuscript was written by YL and all authors commented on previous versions of the manuscript. All authors read and approved the final manuscript.

**Funding** Funding for James E. Hawkins came from the Doctoral Training Centre, Soft Matter for Formulation and Industrial Innovation, grant EP/S023631/1.

**Availability of data and materials** The datasets generated during and/or analysed during the current study are available at <https://doi.org/10.5518/881>

**Code availability** Not applicable.

**Compliance with ethical standards**

**Conflicts of interest** The authors declare that they have no conflict of interest.

**Open Access** This article is licensed under a Creative Commons Attribution 4.0 International License, which permits use, sharing, adaptation, distribution and reproduction in any medium or format, as long as you give appropriate credit to the original author(s) and the source, provide a link to the Creative Commons licence, and indicate if changes were made. The images or other third party material in this article are included in the article's Creative Commons licence, unless indicated otherwise in a credit line to the material. If material is not included in the article's Creative Commons licence and your intended use is not permitted by statutory regulation or exceeds the permitted use, you will need to obtain permission directly from the copyright holder. To view a copy of this licence, visit <http://creativecommons.org/licenses/by/4.0/>.

## References

- Barbosa I, Merquior D, Peixoto F (2005) Continuous modelling and kinetic parameter estimation for cellulose nitration. *Chem Eng Sci* 60:5406–5413. <https://doi.org/10.1016/j.ces.2005.05.029>
- Brehm M, Pulst M, Kressler J, Sebastiani D (2019) Triazolium-based ionic liquids: a novel class of cellulose solvents. *J Phys Chem B* 123:3994–4003. <https://doi.org/10.1021/acs.jpcc.8b12082>
- Budtova T, Navard P (2015) Viscosity-temperature dependence and activation energy of cellulose solutions. *Nord Pulp Pap Res J* 30:99–104. <https://doi.org/10.3183/npprj-2015-30-01-p099-104>
- Cai J, Wang L, Zhang L (2007) Influence of coagulation temperature on pore size and properties of cellulose membranes prepared from NaOH–urea aqueous solution. *Cellulose* 14:205–215. <https://doi.org/10.1007/s10570-007-9106-3>
- Chen F, Sawada D, Hummel M, Sixta H, Budtova T (2020) Swelling and dissolution kinetics of natural and man-made cellulose fibers in solvent power tuned ionic liquid. *Cellulose* 27:7399–7415. <https://doi.org/10.1007/s10570-020-03312-5>
- Cho HM, Gross AS, Chu J-W (2011) Dissecting force interactions in cellulose deconstruction reveals the required solvent versatility for overcoming biomass recalcitrance. *J Am Chem Soc* 133:14033–14041. <https://doi.org/10.1021/ja2046155>
- Clotworthy H (1928) The manufacture of artificial silk with special reference to viscose. *J Soc Chem Ind* 47:24–30. <https://doi.org/10.1002/jctb.5000470202>
- Cuissinat C, Navard P, Heinze T (2008) Swelling and dissolution of cellulose Part IV: free floating cotton and wood fibres in ionic liquids. *Carbohydr Polym* 72:590–596. <https://doi.org/10.1016/j.carbpol.2007.09.029>
- Druel L, Niemeyer P, Milow B, Budtova T (2018) Rheology of cellulose-[DBNH][CO 2 Et] solutions and shaping into aerogel beads. *Green Chem* 20:3993–4002. <https://doi.org/10.1039/C8GC001189C>
- El Seoud OA, Koschella A, Fidale LC, Dorn S, Heinze T (2007) Applications of ionic liquids in carbohydrate chemistry: a window of opportunities. *Biomacromol* 8:2629–2647. <https://doi.org/10.1021/bm070062i>
- Fox SC, Li B, Xu D, Edgar KJ (2011) Regioselective esterification and etherification of cellulose: a review. *Biomacromol* 12:1956–1972. <https://doi.org/10.1021/bm200260d>
- Gericke M, Schluffer K, Liebert T, Heinze T, Budtova T (2009) Rheological properties of cellulose/ionic liquid solutions: from dilute to concentrated states. *Biomacromol* 10:1188–1194. <https://doi.org/10.1021/bm801430x>
- Gindl W, Keckes J (2005) All-cellulose nanocomposite. *Polymer* 46:10221–10225. <https://doi.org/10.1016/j.polymer.2005.08.040>
- Glasser WG et al (2012) About the structure of cellulose: debating the Lindman hypothesis. *Cellulose* 19:589–598. <https://doi.org/10.1007/s10570-012-9691-7>
- Graenacher C (1934) Cellulose solution. U.S. Patent 1943176
- Green SM, Ries ME, Moffat J, Budtova T (2017) NMR and rheological study of anion size influence on the properties of two imidazolium-based ionic liquids. *Sci Rep* 7:8968. <https://doi.org/10.1038/s41598-017-09509-2>
- Gupta KM, Hu Z, Jiang J (2013) Molecular insight into cellulose regeneration from a cellulose/ionic liquid mixture: effects of water concentration and temperature. *RSC Adv* 3:4425–4433. <https://doi.org/10.1039/C3RA22561E>
- Hawkins J, Ries ME, Hine PJ (2020) Carbohydrate polymer technologies and applications, submitted for publication

- Heinze T, Schwikal K, Barthel S (2005) Ionic liquids as reaction medium in cellulose functionalization. *Macromol Biosci* 5:520–525. <https://doi.org/10.1002/mabi.200500039>
- Huber T, Müssig J, Curnow O, Pang S, Bickerton S, Staiger MP (2012) A critical review of all-cellulose composites. *J Mater Sci* 47:1171–1186. <https://doi.org/10.1007/s10853-011-5774-3>
- Jiang ZM, Tang L, Gao X, Zhang WT, Ma JW, Zhang LP (2019) Solvent regulation approach for preparing cellulose-nanocrystal-reinforced regenerated cellulose fibers and their properties. *ACS Omega* 4:2001–2008. <https://doi.org/10.1021/acsomega.8b03601>
- Le KA, Rudaz C, Budtova T (2014) Phase diagram, solubility limit and hydrodynamic properties of cellulose in binary solvents with ionic liquid. *Carbohydr Polym* 105:237–243. <https://doi.org/10.1016/j.carbpol.2014.01.085>
- Lindman B, Karlström G, Stigsson L (2010) On the mechanism of dissolution of cellulose. *J Mol Liq* 156:76–81. <https://doi.org/10.1016/j.molliq.2010.04.016>
- Liu H, Cheng G, Kent M, Stavila V, Simmons BA, Sale KL, Singh S (2012) Simulations reveal conformational changes of methylhydroxyl groups during dissolution of cellulose I $\beta$  in ionic liquid 1-ethyl-3-methylimidazolium acetate. *J Phys Chem B* 116:8131–8138. <https://doi.org/10.1021/jp301673h>
- Lovell CS, Walker A, Damion RA, Radhi A, Tanner SF, Budtova T, Ries ME (2010) Influence of cellulose on ion diffusivity in 1-ethyl-3-methyl-imidazolium acetate cellulose solutions. *Biomacromolecules* 11:2927–2935. <https://doi.org/10.1021/bm1006807>
- Lu B, Xu A, Wang J (2014) Cation does matter: how cationic structure affects the dissolution of cellulose in ionic liquids. *Green Chem* 16:1326–1335. <https://doi.org/10.1039/C3GC41733F>
- Matsumoto T, Tatsumi D, Tamai N, Takaki T (2001) Solution properties of celluloses from different biological origins in LiCl-DMAC. *Cellulose* 8:275–282. <https://doi.org/10.1023/A:1015162027350>
- Moon RJ, Martini A, Nairn J, Simonsen J, Youngblood J (2011) Cellulose nanomaterials review: structure, properties and nanocomposites. *Chem Soc Rev* 40:3941–3994. <https://doi.org/10.1039/C0CS00108B>
- Nishino T, Takano K, Nakamae K (1995) Elastic modulus of the crystalline regions of cellulose polymorphs. *J Polym Sci, Part B: Polym Phys* 33:1647–1651. <https://doi.org/10.1002/polb.1995.090331110>
- Nishino T, Matsuda I, Hirao K (2004) All-cellulose composite. *Macromolecules* 37:7683–7687. <https://doi.org/10.1021/ma049300h>
- Parviainen H et al (2014) Dissolution enthalpies of cellulose in ionic liquids. *Carbohydr Polym* 113:67–76. <https://doi.org/10.1016/j.carbpol.2014.07.001>
- Polyuto A, Kleiner YY, Irklei V, Gal'braikh L (2000) Study of the possibility of processing cotton cellulose in bulk for fabrication of viscose fibre. *Fibre Chem* 32:353–355. <https://doi.org/10.1023/A:1004111809504>
- Ratanakamnuan U, Atong D, Aht-Ong D (2012) Cellulose esters from waste cotton fabric via conventional and microwave heating. *Carbohydr Polym* 87:84–94. <https://doi.org/10.1016/j.carbpol.2011.07.016>
- Ries ME, Radhi A, Keating AS, Parker O, Budtova T (2014) Diffusion of 1-ethyl-3-methyl-imidazolium acetate in glucose, cellobiose, and cellulose solutions. *Biomacromolecules* 15:609–617. <https://doi.org/10.1021/bm401652c>
- Rosenau T, Pothast A, Adorjan I, Hofinger A, Sixta H, Firgo H, Kosma P (2002) Cellulose solutions in N-methylmorpholine-N-oxide (NMMO)-degradation processes and stabilizers. *Cellulose* 9:283–291. <https://doi.org/10.1023/A:1021127423041>
- Sayyed AJ, Deshmukh NA, Pinjari DV (2019) A critical review of manufacturing processes used in regenerated cellulosic fibres: viscose, cellulose acetate, cuprammonium LiCl/DMAC, ionic liquids, and NMMO based lyocell. *Cellulose* 26:2913–2940. <https://doi.org/10.1007/s10570-019-02318-y>
- Sen S, Martin JD, Argyropoulos DS (2013) Review of cellulose non-derivatizing solvent interactions with emphasis on activity in inorganic molten salt hydrates. *ACS Sustain Chem Eng* 1:858–870. <https://doi.org/10.1021/sc400085a>
- Sescousse R, Le KA, Ries ME, Budtova T (2010) Viscosity of celluloseimidazolium-based ionic liquid solutions. *J Phys Chem B* 114:7222–7228. <https://doi.org/10.1021/jp1024203>
- Swatloski RP, Spear SK, Holbrey JD, Rogers RD (2002) Dissolution of cellulose with ionic liquids. *J Am Chem Soc* 124:4974–4975. <https://doi.org/10.1021/ja025790m>
- Zhang JM, Wu J, Yu J, Zhang XY, He JS, Zhang J (2017) Application of ionic liquids for dissolving cellulose and fabricating cellulose-based materials: state of the art and future trends. *Mater Chem Front* 1:1273–1290. <https://doi.org/10.1039/C6QM00348F>

**Publisher's Note** Springer Nature remains neutral with regard to jurisdictional claims in published maps and institutional affiliations.